Available online at www.sciencedirect.com
ScienceDirect
Combustion and Flame 151 (2007) 665–675
Combustion and Flame
www.elsevier.com/locate/combustflame

# Radiative extinction of gaseous spherical diffusion flames in microgravity

K.J. Santa [a], B.H. Chao [a], P.B. Sunderland [b], D.L. Urban [c], D.P. Stocker [c], R.L. Axelbaum [d,*]

[a] *Department of Mechanical Engineering, University of Hawaii at Manoa, Honolulu, HI 96822, USA*
[b] *Department of Fire Protection Engineering, University of Maryland, College Park, MD 20742, USA*
[c] *NASA Glenn Research Center, Cleveland, OH 44135, USA*
[d] *Department of Mechanical and Aerospace Engineering, Washington University, St. Louis, MO 63130, USA*

Received 23 November 2006; received in revised form 27 July 2007; accepted 15 August 2007

Available online 23 October 2007

**Abstract**

Radiative extinction of spherical diffusion flames was investigated experimentally and numerically. The experiments involved microgravity spherical diffusion flames burning ethylene and propane at 0.98 bar. Both normal (fuel flowing into oxidizer) and inverse (oxidizer flowing into fuel) flames were studied, with nitrogen supplied to either the fuel or the oxygen. Flame conditions were chosen to ensure that the flames extinguished within the 2.2 s of available test time; thus extinction occurred during unsteady flame conditions. Diagnostics included color video and thin-filament pyrometry. The computations, which simulated flow from a porous sphere into a quiescent environment, included detailed chemistry, transport, and radiation and yielded transient results. Radiative extinction was observed experimentally and simulated numerically. Extinction time, peak temperature, and radiative loss fraction were found to be independent of flow rate except at very low flow rates. Radiative heat loss was dominated by the combustion products *downstream* of the flame and was found to scale with flame surface area, not volume. For large transient flames the heat release rate also scaled with surface area and thus the radiative loss fraction was largely independent of flow rate. Peak temperatures at extinction onset were about 1100 K, which is significantly lower than for kinetic extinction. An important observation of this work is that while radiative heat losses can drive transient extinction, this is not only because radiative losses are increasing with time but also because the heat release rate is falling off as the flame expands away from the burner and the reactant supply to the flame decreases.


*Keywords:* Extinction; Microgravity; Laminar diffusion flames; CFD; Thin-filament pyrometry

## 1. Introduction

Diffusion flame extinction is of both fundamental and practical interest. Extinction is important to applications such as fire safety, quenching near solid boundaries, and flame anchoring in burners. Flame

* Corresponding author. Fax: +1 314 935 7211.
*E-mail address:* rla@wustl.edu (R.L. Axelbaum).

0010-2180/$ – see front matter 
doi:10.1016/j.combustflame.2007.08.009

extinction can be characterized as either kinetic (i.e., diffusive) or radiative. Kinetic extinction occurs at short residence times (i.e., at high strain rates or scalar dissipation rates), whereas radiative extinction is expected at long residence times. Kinetic extinction can readily be observed experimentally, such as in counterflow flames when strain rate is increased to the point of extinction, and this has been extensively studied [1–3]. On the other hand, radiative extinction, which was theoretically predicted by Chao et al. [4] for droplet burning, is much more difficult to observe, and researchers have been seeking compelling experimental evidence for this phenomenon. Radiative extinction occurs at very low strain rates and for this reason it is of particular interest for spacecraft fire safety, where buoyancy is not available to accelerate (strain) the flow field.

Radiative extinction of spherical diffusion flames, whether droplet or burner-supported, is predicted by a simple scaling analysis. Because the radiative heat loss is a temperature-sensitive volumetric loss mechanism, the loss rate depends on the volume of the high-temperature region, which is given by $(4\pi/3)(r_o^3 - r_i^3)$, where $r_o$ and $r_i$ are, respectively, the outer and inner radii of the radiation region. Taking $r_o = r_i + \Delta r$, for large flames with $r_i \gg \Delta r$, the volume is reduced to $4\pi r_f^2\, \Delta r$, where the flame radius $r_f$ is approximated by $r_i$. The radiative loss rate then scales with flame surface area (i.e., the square of the flame radius) times the thickness of the high-temperature zone. This thickness is independent of flame radius in the limit of large flames (although it increases with flame radius for small flames) [4]. Thus, for large flames, radiation scales with radius squared. For small flames where $\Delta r$ is not small compared to $r_f$, it is dependent on $r_f$ and the radiative heat loss scales with radius raised to a power of between 2 and 3. On the other hand, both the heat release rate and the flame radius of quasi-steady flames are proportional to the reactant flow rate [5,6]. Thus, in large quasi-steady flames, the radiative heat loss fraction scales with flame radius (for small flames it scales with radius raised to the power of between 1 and 2). For radiative extinction to occur, the rate of radiative heat loss must be comparable to the rate of heat release, and since for large microgravity flames this ratio scales with radius, radiative extinction is possible for these flames.

Radiative extinction is unlikely in normal gravity because buoyancy increases with flame size, and under conditions where radiative extinction might otherwise occur, buoyancy enhances mixing and reduces residence times. On the other hand, radiative extinction can be important in microgravity and an improved understanding of this phenomenon could contribute to spacecraft fire safety. Microgravity experiments allowed the first observation of radiative extinction, this being for droplet combustion [7,8]. Extinction occurred for quasi-steady burning of large droplets, for which flame radius is proportional to droplet radius and the above scaling predicts large radiative loss fractions. Radiative extinction has also been reported for counterflow flames in microgravity [9].

Radiative extinction also is possible in burner-supported spherical diffusion flames. For quasi-steady burning, flame radius is proportional to reactant flow rate [6,10]. As the above scaling indicates, at high enough reactant flow rates, radiative extinction is possible. Radiative extinction was experimentally observed in microbuoyant burner-supported spherical flames in normal gravity by Yoo et al. [11], but these were not truly nonbuoyant flames and a small amount of buoyancy can have a significant impact on flames near extinction. Tse et al. [12] numerically predicted radiative extinction in burner-supported spherical flames but were not able to observe extinction experimentally. Other theoretical investigations on spherical flames are reported in King [13], Atreya and Agrawal [14], Mills and Matalon [6,15], Christiansen et al. [16], and Liu et al. [10].

The time required to obtain steady-state spherical flames is typically on the order of tens of seconds. This precludes the observation of quasi-steady extinction in ground-based facilities. On the other hand, transient extinction can be observed. The experiments described here seek to understand radiative extinction in transient spherical diffusion flames. Unlike droplet burning, the flow fields in these flames are steady and the unsteadiness is primarily a consequence of the evolving thermal and concentration fields. In addition, since gaseous fuels are used, the stoichiometric mixture fraction can be easily varied by varying the fuel concentration.

## 2. Experimental

The experiments were conducted in microgravity in the NASA Glenn 2.2-s drop tower. The experimental apparatus is described in detail in Sunderland et al. [17,18]. The burner reactant flows from a storage tank through a solenoid valve, a metering valve, a mass flowmeter, and a second solenoid valve into the spherical burner. As before, the burner is a 6.4-mm-diameter porous stainless-steel sphere. All tests were conducted in a pressure vessel of 26 L initially at room temperature and 0.98 bar (with an estimated uncertainty of ±0.005 bar). Flames were ignited immediately after drop initiation by a hot wire.

The present tests involved either ethylene (99.9% purity) or propane (99.9% purity) as fuel, as well as

oxygen (99.999% purity) and nitrogen (99.999% purity). Gas mixtures were prepared by partial-pressure mixing. The estimated composition uncertainty of the mixtures was ±0.001 mole fraction. Both normal and inverse flames were considered here. In normal flames the pressure vessel contained an atmosphere of oxidizer, while in inverse flames the atmosphere contained fuel [17,18]. Various levels of nitrogen dilution were considered to obtain conditions where flames would ignite and then extinguish within the 2.2 s of available microgravity time.

The flow rate for the burner-side reactant was calibrated in steady state in normal gravity. The pressure drop across the porous burner caused unsteady burner flow rates after flow commenced. To minimize these transients, a pressure transducer was installed just upstream of the burner, its output was recorded at 170 Hz during each test, and care was taken to maintain a nearly constant pressure at this location. This was accomplished by opening the first solenoid valve for a predetermined interval (0.25–4 s, optimized for each test condition) about 20 s prior to drop initiation to pressurize the plumbing system between the solenoid valves. At 1 s before drop initiation, both solenoid valves were opened to commence flow. During burn tests, the transducer indicated pressure drops across the burner of 0.03–1.86 bar, corresponding to the lowest and highest steady-state flow rates considered here. This pressure drop was held constant within 10% during each test. Thus uncertainties in the flow rates are estimated at ±15%.

The flames were imaged using a color charge-coupled device (CCD) video camera with 8- and 16-mm manual-iris lenses at $f$ 1.4. Spatial resolution was 0.2 and 0.1 mm, respectively. Flame diameters were measured using the contours of peak blue emission in the video record. Diameters were determined by averaging the longest chord through each flame and its perpendicular chord.

Two modes of extinction onset were observed: base and hole extinction. Base extinction, typically observed at small flow rates, started at the base of the flame near the burner supply tube. Hole extinction, typically observed at high flow rates, started as a flame hole in the blue flame sheet at a distance away from the burner tube. Such holes grew with time. Base or hole extinction often led to complete extinction, where all blue-flame luminosity disappeared during a drop test. For flames in which base extinction was observed, extinction time is reported as the time when 50% of the previously visible flame surface (as viewed by the video camera) was no longer visible. For flames in which hole extinction was observed, extinction time is reported as the time when a hole was first visible. Extinction times reported here are referenced to the time datum at ignition. For some tests, a resistively heated wire was placed around the burner tube and was energized (in microgravity) to help prevent base extinction.

Approximate peak temperatures were measured using thin-filament pyrometry, a technique pioneered by Villimpoc and Goss [19]. Similarly to the work of [20], four SiC fibers with diameters of 13.9 μm were strung across the flames in the focal plane of a Nikon D100 digital single-lens reflex camera. This color camera has 3008 × 2000 pixels and 12 bits per color plane and is similar to the still camera used by [21] for soot pyrometry. The tests were conducted with a 60-mm lens at $f$ 4, a shutter time of 33 ms, a detector sensitivity of ISO 800, a white balance of direct sunlight, and with all automatic gain and focusing disabled. This diagnostic was developed and calibrated in the range 1400–2200 K using thermocouples in a normal-gravity methane/air flame [22]. For longer exposures similar to those used in the present work, a measurement threshold of 800 K was found [22]. A solenoid triggered the shutter release, whereby the camera recorded four images per drop test. There was no saturation in the images in any color plane. The images were converted to grayscale (with a range of 0–4095) and smoothed using 5 × 5 pixel binning. The brightest smoothed pixel grayscale was recorded along each of the eight fiber-flame crossings and these were averaged. The results were converted to relative peak fiber temperatures using the system calibration of 0.215 K/grayscale [22]. These temperatures have an estimated uncertainty of ±25 K. These temperatures were offset and radiation corrections were applied to determine peak gas temperatures. The offset was chosen iteratively such that the measured and predicted peak gas temperatures matched at a particular time and condition (0.7 s and 5.1 mg/s). The radiative loss from these fibers in the present flames, based on a fiber temperature of 1400 K, is estimated at 0.3 W.

## 3. Numerical

For the numerical simulation, a gaseous reactant is injected from the porous spherical burner at a surface temperature of $T_b$ into a nearly infinite quiescent environment of the other reactant at a temperature of $T_\infty$. The burner is assumed to be perfectly symmetric, so that the flow field and flame are spherically symmetric. Following the work of Tse et al. [12], the numerical code is a modification of the PREMIX [23] code, adapted to a diffusion flame in a spherical geometry and allowing for optically thick radiative heat losses. For this problem, the equations describing the conservation of mass, energy, and gas species are,

$$\frac{\partial \rho}{\partial t} + \frac{1}{r^2}\frac{\partial (r^2 \rho u)}{\partial r} = 0, \tag{1}$$

$$\rho c_p \frac{\partial T}{\partial t} = \frac{1}{r^2}\frac{\partial}{\partial r}\left(r^2 \lambda \frac{\partial T}{\partial r}\right) - \rho u c_p \frac{\partial T}{\partial r} - \sum_{k=1}^{K}\left(\rho c_{p,k} Y_k V_k \frac{\partial T}{\partial r} + h_k \omega_k Y_k\right) - \mathrm{Ra}, \tag{2}$$

$$\rho \frac{\partial Y_k}{\partial t} = -\frac{1}{r^2}\frac{\partial}{\partial r}\left(r^2 \rho Y_k V_k\right) - \rho u \frac{\partial Y_k}{\partial r} + W_k \omega_k Y_k, \quad k = 1, 2, \ldots, K, \tag{3}$$

where $T$ is the temperature, $Y_k$ is the mass fraction of species $k$, $W_k$ is the molecular weight of species $k$, $t$ is time, $r$ is the radial spatial coordinate, $u$ is the radial flow velocity, $\rho$ is the gas density, $c_p$ is the averaged specific heat at constant pressure, $\lambda$ is the heat conductivity, $h_k$ is the specific enthalpy of species $k$, $c_{p,k}$ is the specific heat of species $k$, $V_k$ is the diffusion velocity of species $k$, $\omega_k$ is the production rate of species $k$, $K$ is the number of species, and Ra is the rate of radiative heat loss. The equations were solved subject to the boundary conditions

$$r = r_b : T = T_b;$$
$$Y_k(u + V_k)u Y_{b,0}, \quad k = 1, 2, \ldots, K, \tag{4}$$
$$r \to \infty : T \to T_\infty;$$
$$Y_k \to Y_{k,\infty}, \quad k = 1, 2, \ldots, K, \tag{5}$$

where the subscripts 0, b, and $\infty$ refer to conditions at the center of the burner, the burner surface, and the ambient, respectively. Burner surface temperature $T_b$ was taken to be constant, since thermocouple measurements of the burner surface in the 2.2-s drop facility showed no significant increase in temperature for the flames considered. In addition, the results indicate that after 5 s the thermal field had only reached a radius of 9 cm from the center of the burner and the computations predicted no significant change in reactant compositions at a radius of 100 cm. Thus, although a finite domain ($r_{wall} = 100$ cm) was used in the computations, it was effectively infinite and the results were not affected by an increase in domain size. Both $T_b$ and $T_\infty$ were taken to be 300 K in this study.

Tse et al. [12] have shown that reabsorption of radiative emission is significant in spherical microgravity flames. Radiation therefore was considered to be optically thick and caused by the participation of $CO_2$, $H_2O$, and CO. The radiative properties of these gases were formulated by a statistical narrow-band model with a spectral bandwidth of 25 $cm^{-1}$. The emissivities were extracted from the line-by-line values given by the HITRAN database [24]. To account for the angular variation of the radiation intensity, the discrete ordinates method was employed, with a discrete representation that included 20 different directions. The rate of radiative heat transfer was then evaluated by integrating over all directions using Gaussian quadrature. A more detailed description of the radiation model can be found in Carlson and Lathrop [25].

Conventional finite difference techniques with nonuniform mesh spacing were adopted for the discretization of the differential equations. The transient terms were expressed by a forward difference formula, the diffusive terms by a central difference formula, and, for better convergence, the convective terms by an upwind difference formula. The discretized equations were solved by Sandia's Twopnt package [26], which uses Newton's method to solve transient and steady-state boundary value problems. The chemical reaction rates, the thermodynamic properties, and the transport properties were evaluated by Chemkin and Transport software [27,28]. The kinetics data were provided by GRI-Mech 3.0, which contains 53 species and 325 reactions [29]. The number of grids was varied until the solution did not change with further addition of grids. The time step was adjusted until the solution converged. GRI-Mech 3.0 has been employed to study steady burning and extinction of ethane and ethylene flames, showing reasonable agreement with experiments [3,20].

## 4. Results and discussion

Fig. 1 illustrates a sequence of images during a drop wherein *hole* extinction is seen to occur. Ignition occurs approximately 30 ms after the release of the rig and the onset of microgravity. The flame is evident as a faint blue line surrounding the porous sphere. Soot produced during the early stages is trapped thermophoretically within the flame and can be seen as the yellow luminous region around the porous sphere. The glow of the heating wire is visible at the bottom. For this flame, propane is flowing into an atmosphere of 17% oxygen. After about 1.5 s, a hole is observed in the outer flame zone between 10 and 12 o'clock. The blue flame is not visible at this location, indicating hole extinction. Soon thereafter the flame extinguishes completely and only luminous emission from residual soot is visible. The asymmetry of the luminosity from the residual soot is likely due to the ignition process, as the blue flame is not asymmetric, as seen in Fig. 1 for earlier times. Also, when the flame extinguishes, there are asymmetries in the thermophoretic force and thus the asymmetry in the soot field grows quickly following extinction (cf. $t = 2.1$ s).

Fig. 2 illustrates *base* extinction for propane flowing into air at 0.75 mg/s with and without the heating wire. Extinction occurs near the burner supply tube at about 1.35 s for both cases, indicating that the time to

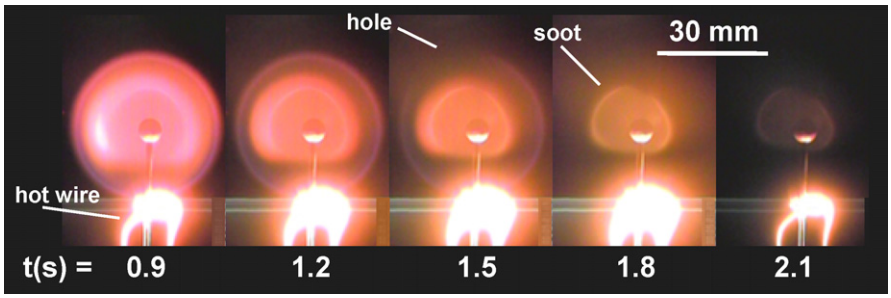


Fig. 1. Time sequence of color images of an extinguishing flame of propane flowing into 17% oxygen at 1.35 mg/s. The round blue region is the flame sheet, the kidney-shaped yellow region is soot, and the white region is a heating wire. The spherical burner and supply tube also are visible here. The heating wire encircles the supply tube to minimize heat loss to the tube. Hole extinction occurred at 1.47 s and complete extinction occurred by 1.8 s. (For interpretation of the references to color in this figure legend, the reader is referred to the web version of this article.)

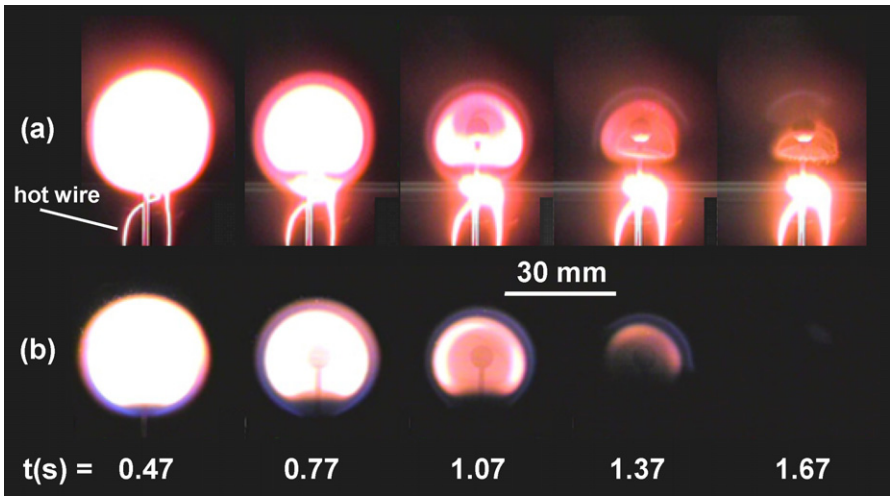


Fig. 2. Time sequences of color images of extinguishing flames of propane flowing into air at 0.75 mg/s (a) with heating wire and (b) without heating wire. The visible features are similar to those described in the caption of Fig. 1. Extinction occurred at the base (base extinction) at 1.37 and 1.33 s, respectively. (For interpretation of the references to color in this figure legend, the reader is referred to the web version of this article.)

extinction is not significantly influenced by heat loss to the burner supply tube. This finding was repeatable and was also supported by results at 1.2 mg/s. It might be expected that instability at the "bottom" of the flame, due to the edge flame, would shift the extinction limits, but this is not the case. The edge flame and unburned region at the supply tube apparently do not influence the bulk of the flame. For this reason it was assumed that base extinction is an appropriate indicator of extinction, within the experimental uncertainties, and thus most tests were performed without the heating wire.

As these drop tower experiments are intrinsically transitory, a transient numerical scheme was used to study the flames. Before comparing the numerical and experimental results, we will discuss the numerical simulations. There are two important considerations with respect to accuracy: convergence, which is dependent on grid spacing, and the initial condition. The former was addressed in this study by varying the grid spacing and domain size to ensure that the results were not dependent on them. The latter is more complicated, because it is impossible to know what the true initial conditions are. Experimentally the flow through the porous sphere begins about 2 s before ignition. Under these conditions one would expect that there is a temporary premixed flame that quickly transitions to a diffusion flame. The critical feature of this ignition is that there is an almost instantaneous establishment of a diffusion flame at some distance from the burner. This fledgling diffusion flame will have steep gradients on either side of the flame. To simulate

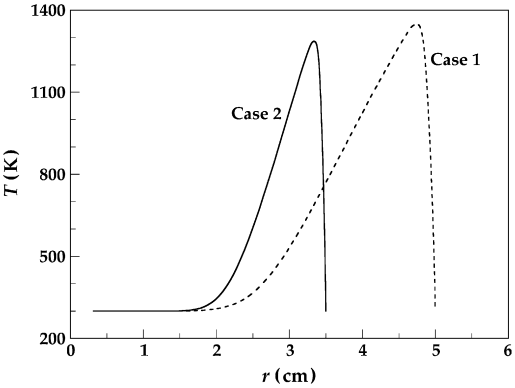


Fig. 3. Modeled radial temperature profiles for two initial conditions for a flame of oxygen flowing into 4% ethylene at 104 mg/s. The two cases are steady-state solutions without radiation and with outer boundaries at 5 cm (case 1) and 3.5 cm (case 2) from the center of the burner.

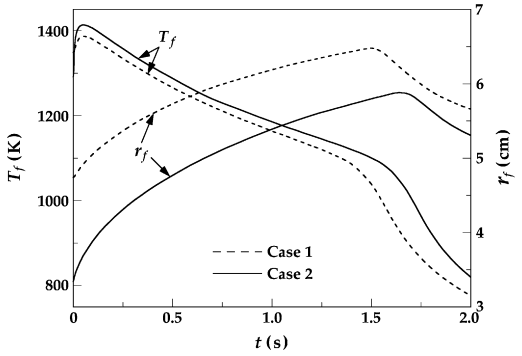


Fig. 4. Modeled evolution of peak temperature and radius for flames of oxygen flowing into 4% ethylene at 104 mg/s for the two initial conditions of Fig. 3. Extinction begins when the flame radius starts to decrease. Cases shown are for a high flow rate with negligible burner heat loss.

this ignition process we have followed the approach of Tse et al. [12] to obtain our initial condition. In this approach the initial condition is given by the compressed steady-state solution of the same flame, which is obtained by forcing the outer boundary closer to the porous sphere. In this way we produce a thin flame with a composition that is similar to what would be expected for the actual flame. In addition, since the flame is very thin compared to the emission (or absorption) length scale of radiation immediately after ignition, radiative losses are negligible, and so radiation is turned off to obtain the steady-state compressed solution. This solution is then used as the ignition source.

Fig. 3 shows temperature profiles for two different initial conditions at different levels of compression, with the outer boundary at 5 cm (case 1) and 3.5 cm (case 2) from the center of the burner, for oxygen issuing into 4% ethylene at 104 mg/s. Fig. 4 illustrates the evolution of the peak temperature and flame radius for the two different initial conditions of Fig. 3. The general characteristics of the flame history include an initial increase in temperature for less than 0.1 s, followed by a gradual reduction in temperature until extinction, which occurs at 1.50 s for case 1 and 1.64 s for case 2. The flame radius, which is defined in this study as the radius of peak temperature, increases until extinction, at which time it shrinks. The two different initial conditions of Fig. 3 lead to nearly identical extinction flame temperatures. The results indicate a shorter extinction time for the larger initial flame (case 1). The high flow rate of 104 mg/s was selected in this demonstration to clearly illustrate the differences.

The basic trends of these results are similar to those of Tse et al. [12] in that radiative losses appear to dominate the flame, leading to a continuous reduction in flame temperature and, given enough time, flame extinction. The initial temperature rise ($t < 0.1$ s) occurs because in the compressed solution, although there is no radiative heat loss, there is significant heat loss to the "outer wall," i.e., the ambient gas (as seen in Fig. 3). This yields a peak temperature for the compressed solution (initial condition) that is less than the early peak temperature of the actual flame (which does not suffer from wall loss). Thus, upon ignition, there is an immediate and momentary rise in flame temperature until radiative losses increase and the temperature begins to decrease. As seen in Fig. 4, case 1 has a lower maximum temperature and extinguishes earlier than case 2 because the compressed flame is larger (see Fig. 3) and thus after ignition the flame suffers more radiative loss. The mass flow rate of these flames is sufficiently high so that there is no conductive loss to the burner, as evidenced by a negligible temperature gradient near the burner.

We use maximum flame radius to define predicted extinction because when the flame extinguishes the location of the peak temperature stops growing and the flame stops consuming reactants (recall that the flame radius is defined as the location of peak temperature). After heat release ceases (i.e., after extinction), heat dissipation causes the maximum temperature and its distance from the burner to decrease. As revealed in Fig. 4, the maximum flame radius provides a more sensitive indication of extinction than the corresponding temperature drop.

The criterion employed for identifying appropriate initial conditions was to compress the initial condition until further compression would prevent ignition, presumably because the heat loss to the "outer wall" was too great. Maximum compression minimizes gaseous radiation by minimizing the volume of radiating species. Following this approach, the maxi-

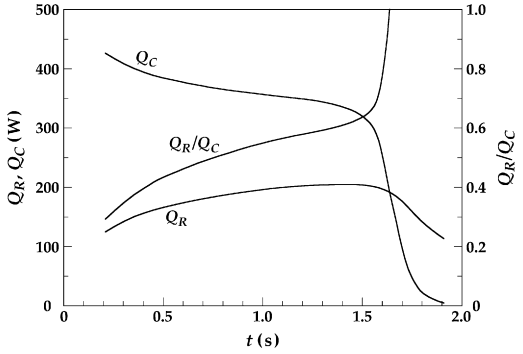


Fig. 5. Modeled radiation loss rate ($Q_R$), heat release rate ($Q_C$), and $Q_R/Q_C$ as a function of time for case 2 of Figs. 3 and 4.

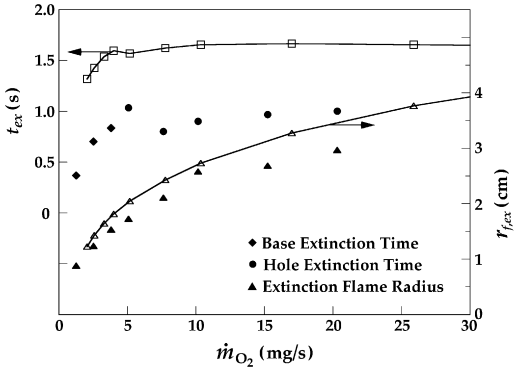


Fig. 6. Measured and predicted extinction times and extinction radii for flames of oxygen flowing into 4% ethylene. No heating wire was used. Open symbols represent numerical extinction.

mum temperature after ignition was found to be similar for all flow rates, except for cases where the flame suffered from burner heat loss, as will be discussed below.

In Fig. 5 the net radiative heat loss rate ($Q_R$), the total heat release rate ($Q_C$), and $Q_R/Q_C$ are plotted versus time for case 2 of Figs. 3 and 4, so that the events leading to extinction can be clearly delineated. $Q_C$ was determined by integrating the local heat release rate over the domain volume, while $Q_R$ was obtained by calculating the net loss rate at the outer boundary of the domain, i.e., $Q_R = 4\pi(r^2 u\,\mathrm{Ra})_{r=r_{wall}}$, because only the heat that leaves the boundary is heat *loss*. While the radiative heat losses increase with time, the increase is rather slow and nearly asymptotes. The heat release rate decreases slowly as well, such that extinction is a consequence of a gradual increase in radiative loss coupled with a gradual decrease in heat release. The flame extinguishes when $Q_R/Q_C$ approaches 0.7, where the temperature is too low to sustain radical production (i.e., $T = T_{ex}$). An interesting feature of this figure is that extinction is not as much driven by a rapid rise in radiative heat loss with time (or flame size) as it is by a reduction in heat release rate with time.

In contrast to extinction at small Damköhler number, the reduction in heat release rate for these flames is due to flame expansion, not reactant leakage resulting from insufficient time for reaction. The results on the reactant profiles at different times show that the leakage of both the ethylene and oxygen across the flame are negligibly small until the flame is about to extinguish. Significant reactant leakage was observed only after flame extinction. Tse et al. [12] also found very little reactant leakage before extinction of spherical flames. As the flame moves away from the burner, less reactant reaches the flame and the heat generation rate reduces with time. The rate of reduction decreases with time because the flame expansion slows down with time.

Experimental and numerical results on flame extinction for oxygen flowing into 4% ethylene are shown in Fig. 6. Two extinction times are shown: base extinction and hole extinction. Both indicate the time after ignition at which extinction is first observed, starting either at the region near the supply tube (base extinction) or elsewhere (hole extinction). At later times the entire flame will extinguish, but the times indicated are representative of the onset of extinction. Also shown is the radius of the flame at extinction. There is satisfactory agreement between experiment and computation for extinction flame radius for the present range of experimental flow rates. Experimental results at higher flow rates were not possible due to flow nonuniformities and the onset of oblong flames. Numerical computations also show that flame size increases with flow rate and that extinction radius roughly scales with the square root of flow rate, which is consistent with Tse et al. [12]. The data in Fig. 6 reveal that the best-fit exponent on flow rate is 0.44. The trends in extinction time with flow rate are similar for experiment and computation. Initially the extinction time increases with flow rate, but at about 10 mg/s it levels off, asymptoting to about 1 s for the experiments and 1.65 s numerically. The shorter extinction time at low flow rate is due to the reduction in flame temperature by burner heat loss. The closer the flame is to the burner, the greater the heat loss to the burner. The temperature is lower and consequently less time is required to reach the extinction temperature. Although burner heat loss affects the time to extinction, it cannot trigger extinction for these flames, because as the flame expands with time, burner heat loss decreases. Instead, extinction is triggered by radiative heat loss, which increases with time. In other words, for the lower flow rate cases, the enthalpy that is removed from the gas mixture due to burner heat loss causes radiative extinction to occur at shorter times.

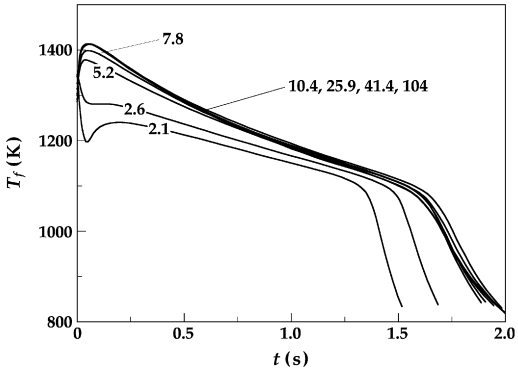


Fig. 7. Modeled flame temperatures for different flow rates of flames of oxygen flowing into 4% ethylene. The curve labels represent oxygen flow rates in mg/s.

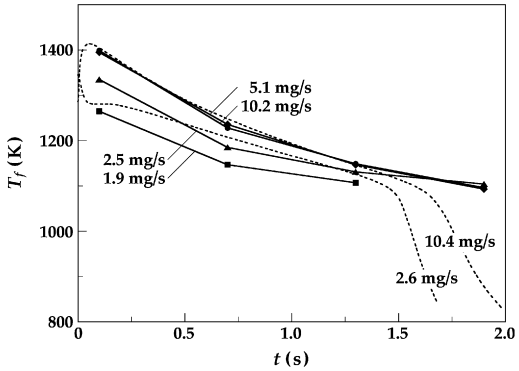


Fig. 8. (—) Pyrometry peak temperatures for flames of oxygen flowing into 5% ethylene. These are nonextinguishing flames except at 1.9 mg/s. Also shown (- - -) are two representative numerical predictions for extinguishing flames of oxygen flowing into 4% ethylene.

The extinction temperature is nearly invariant with flow rate (Fig. 7), even with those flames that suffer from burner heat loss. For the oxygen into 4% ethylene flames the extinction temperature was 1100 K at the lowest flow rates, and it dropped less than 50 K to 1055 K at 104 mg/s. The result is expected, as the chemistry of extinction is controlled by temperature and the basic structure of the flame does not change, particularly since radiative heat loss is volumetric heat loss.

At high flow rates, the results of Fig. 7 are similar to those of Fig. 4, where the temperature first increases slightly and then continuously falls off until extinction at about 1.65 s. Extinction is seen here as a rapid drop in peak temperature, indicating the end of heat generation. For flow rates less than 3 mg/s, a different trend is observed at early times. Here the temperature initially decreases and then increases before it begins its slow decrease to extinction due to radiative heat loss. These conditions indicate burner heat loss for the lower flow rates, and it is evident that the decrease in temperature at early times results in a lower initial temperature and thus a shorter time for extinction. However, for flow rates greater than about 8 mg/s the temperature versus time curves are practically identical.

Thin-filament pyrometry measurements are shown in Fig. 8 for oxygen flowing into 5% ethylene at various flow rates. Fig. 8 also includes representative predictions from Fig. 7 for oxygen flowing into 4% ethylene. The measurements were taken at a slightly higher ethylene concentration to avoid filament-induced extinction. An offset was applied to the filament measurements to force agreement with the predictions at 0.7 s for an oxygen flow rate of 5.1 mg/s. The measurements show that, at any given time, flows greater than 5 mg/s result in peak temperatures that are independent of flow rate, whereas for lower flow rates peak temperatures decrease with decreasing flow rate. This is consistent with the numerical predictions. For a flow rate of 1.9 mg/s the flame extinguishes shortly after 1.35 s. The temperatures could not be obtained after extinction, suggesting that the temperature was below the 800-K pyrometer threshold temperature.

The present results indicate an extinction temperature of about 1100 K for the present flames (Figs. 4, 7 and 8). This is lower than past measurements of this property in normal-gravity flames [30]. For example, Williams [31] indicates an extinction temperature of $1500 \pm 50$ K for hydrocarbon combustion in oxygen/nitrogen mixtures. Macek [32] reports an extinction temperature of 1600 K for both diffusion and premixed flames. The significantly lower temperature at extinction reported here for microgravity diffusion flames is consistent with radiative extinction, as predicted by the analytical study of Chao et al. [4].

Results for extinction time and extinction radius as functions of flow rate for propane flowing into 17% oxygen are shown in Fig. 9. Again, there is satisfactory agreement between experiment and computation for the extinction radius. Nonetheless, the numerical results for extinction time at low flow rates show a trend that does not agree with experiments or the results in Fig. 6. Moreover, the best-fit exponent of flame radius on flow rate is 0.36. In Fig. 9, except for a narrow range of low flow rates, the extinction time predicted by the computations monotonically decreases and asymptotes to 2 s. This result may appear inconsistent with the discussion of Fig. 6 and further study will be necessary to explain this result—but here we will consider the consistent trend for the two cases, that of the asymptotic behavior at large flow rates, indicating that extinction time is independent of flow rate.

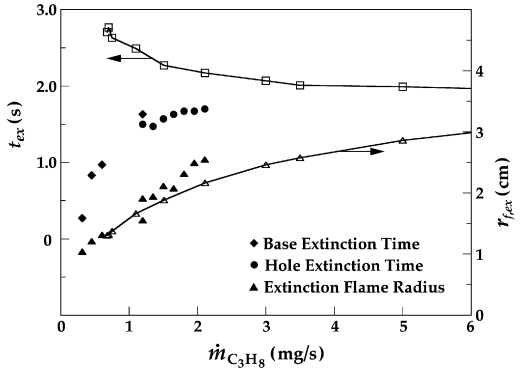


Fig. 9. Measured and predicted extinction times and extinction radii for flames of propane flowing into 17% oxygen. A heating wire was used.

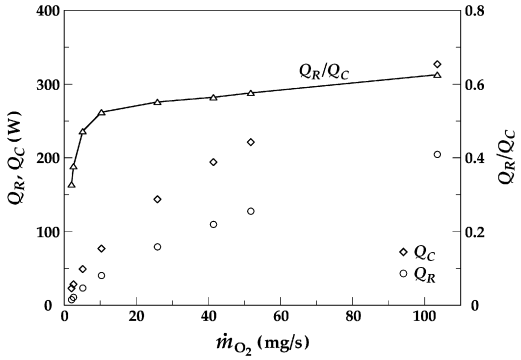


Fig. 10. Modeled radiation loss rate ($Q_R$), heat release rate ($Q_C$), and $Q_R/Q_C$ near extinction for different flow rates plotted versus flow rate. Results shown are for flames of oxygen flowing into 4% $C_2H_4$.

As shown in Figs. 6 and 9, the flame size at extinction increases with flow rate, and thus it might be expected that larger flames would extinguish earlier, because radiative losses would be greater in the larger flames. Indeed, steady-state theories of extinction [4,14,15] indicate that increasing flame size leads to extinction due to the greater radiative losses with flame size. However, as shown in Fig. 10, for these transient flames additional factors must be considered. Here the net radiative heat loss rate ($Q_R$), the total heat release rate ($Q_C$), and $Q_R/Q_C$ are plotted versus oxygen flow rate just before extinction. Clearly, as flow rate and flame radius increase, radiative heat losses increase. But at the same time, $Q_C$ increases because the flame surface area (fuel consumption rate) increases. The plot of $Q_R/Q_C$ indicates that this ratio, which is the primary variable affecting flame extinction, initially increases rapidly with flow rate but then slows dramatically for flow rates above 10 mg/s. This explains why at high flow rates all flames have similar temperature versus time

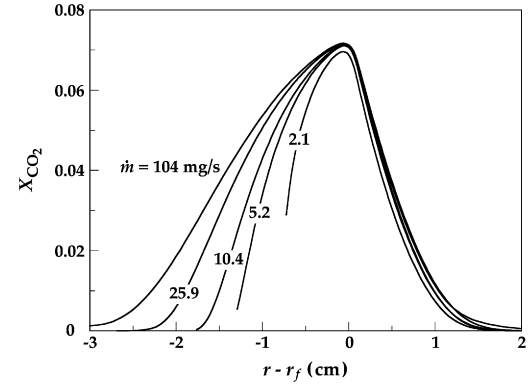


Fig. 11. Modeled mole fraction of $CO_2$ as a function of radius. In these flames oxygen flowed into 4% ethylene in nitrogen at various flow rates. Oxygen flow rates (in mg/s) are labeled for each curve. The curves correspond to times of 0.5 s after ignition. Symbols $r$ and $r_f$ indicate radius and radius at peak temperature, respectively.

relationships (Fig. 7), even though the flame sizes are different. These flames do not experience burner heat loss, and since the ratio of radiative heat loss to heat release is similar for these flames, they experience the same flame temperature history.

While heat release rate increases with flow rate, $Q_R/Q_C$, shown in Fig. 10 increases only slightly for flow rates greater than 10 mg/s. This suggests that for large flames, radiative heat losses scale with surface area, not volume, which is in agreement with our discussion in the Introduction and earlier works [4,12]. To understand this, we have plotted in Fig. 11 the mole fraction of $CO_2$ for the flames of Fig. 6 at 0.5 s after ignition. Both $CO_2$ and water are responsible for radiative heat loss, but we will concentrate on $CO_2$, with the understanding that the key findings will be similar for water vapor. The data are plotted relative to the flame location, i.e., $r - r_f$, where $r$ is the radius and $r_f$ is the flame location. While the thickness of the $CO_2$ layer increases with flow rate on the inside of the flame, it is clear that the thickness outside the flame is nearly constant, and it is this region that dominates the radiative loss from the flame. We can understand this dominance as follows: first, the volume of each layer scales with radius squared, and since the flame exterior has a larger radius than the flame interior, its volume will be considerably greater. Second, since these flames are optically thick, some of the radiation from the inside layer will be trapped by the outside layer and thus will not constitute a "loss."

The invariance in the outer layer thickness for a wide range of flow rates implies that the volume of the radiative zone increases with surface area. This explains why the ratio of $Q_R/Q_C$ starts to level off in Fig. 10, because when heat loss to the burner is negligible, both $Q_R$ and $Q_C$ scale with flame surface area.

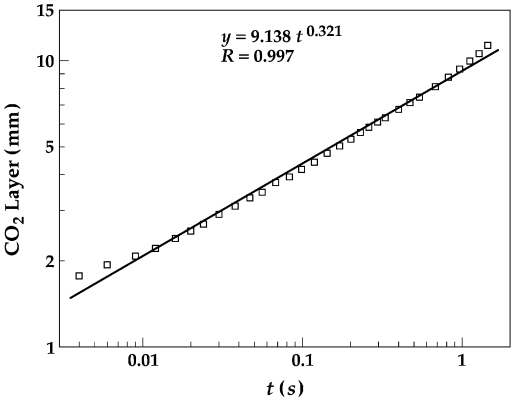


Fig. 12. Thickness of the $CO_2$ layer as a function of time. Thickness is defined as the region where the mole fraction of $CO_2$ drops to 35% of its peak value in the outer layer of the flame. The data shown are for a flame of oxygen issuing into 4% ethylene at 41 mg/s.

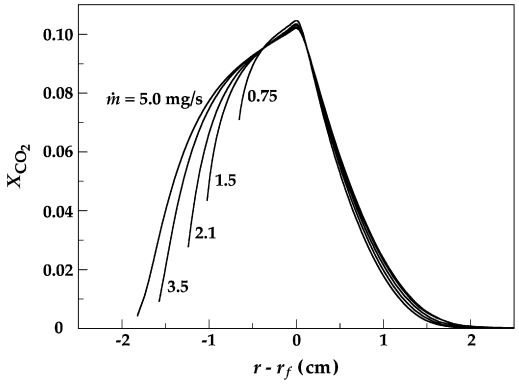


Fig. 13. Comparison of modeled $CO_2$ mole fractions for flames of $C_3H_8$ flowing into 17% $O_2$. Flow rates (in mg/s) are labeled for each curve. The curves correspond to times of 0.5 s after ignition.

With this explanation, it is also clear why radiative losses grow only slowly with time (as seen in Fig. 5).

In the outer layer, the spread rate of the radiating species ($CO_2$ and $H_2O$) is due to diffusion, not mass flow rate, and since there is an infinite domain, there is no characteristic length associated with the spread. Then, from simple scaling laws, we see that the diffusion thickness $\delta$ scales with $(Dt)^{1/2}$, where $D$ is diffusivity and $t$ is time. Approximating $D$ as 1 $cm^2/s$ and $t$ as 0.5 s yields a diffusion thickness on the order of 0.7 cm, which is consistent with the thickness of the outer layer shown in Fig. 11. Fig. 12 shows how the thickness of the $CO_2$ layer in the outer layer varies with time. The power law fit shows the exponent on time is 0.32, which is slightly smaller than the simple estimated value of 0.5. This difference is likely due to the temperature dependence of $D$, which decreases with decreasing temperature.

Fig. 13 shows that $CO_2$ mole fraction profiles for *normal*, low-$Z_{st}$ $C_3H_8$ flames, where the stoichiometric mixture fraction $Z_{st}$ is defined as

$$Z_{st} = Y_{O,b}/(Y_{O,b} + \sigma Y_{F,b}). \quad (6)$$

In Eq. (6), $\sigma = (\nu_O W_O)/(\nu_F W_F)$ is the stoichiometric oxidizer-to-fuel mass ratio, the subscripts "F" and "O" denote fuel and oxidizer, respectively, and the subscript "b" denotes conditions of the reactants at their supply. These results show similar trends to those of Fig. 11, which are for *inverse* high-$Z_{st}$ $C_2H_4$ flames indicates that the general behavior of these flames with flow rate is independent of fuel type and normal versus inverse configuration. This helps explain why these flames have similar extinction times, as shown in Figs. 6 and 9, and is consistent with the diffusion thickness argument for the outer layer discussed above, wherein the diffusion time dominates extinction, and fuel type and flame configuration are of secondary importance.

## 5. Conclusions

Spherical burner-supported diffusion flames were observed and modeled to examine radiative and kinetic extinction during transient burning. The major findings are as follows:

1. Flames were observed that ignited and extinguished within the 2.2-s available test time. Two modes of extinction were identified: base and hole extinction. The onset times of both modes were the same within experimental uncertainties. Predictions indicate that peak temperatures at extinction onset were about 1100 K.
2. The experiments and computations indicate that spherical diffusion flames generally grow and cool after ignition. Except at low flow rates, the peak temperature decreases monotonically with time, but is independent of flow rate.
3. Extinction radius roughly scales with flow rate raised to the 0.4 power.
4. At low flow rates, extinction time increases with flow rate, owing to burner heating effects. At high flow rates, extinction time is relatively independent of flow rate.
5. Radiative heat loss is dominated by the region outside of the flame and thus scales with flame surface area, not flame volume. For large transient flames, heat release rate also scales with surface area, so that radiative loss fraction is relatively independent of flow rate.
6. While radiative heat losses can drive extinction, it is not only because radiative losses are increasing with time (flame size). Rather, the heat release

rate is also decreasing as the flame expands, and it is this combination that leads to extinction.

## Acknowledgments

This work was supported by NASA Grants NCC3-697 and 1063 (RLA), NCC3-696 and 1062 (BHC), and NNC05-AA46A (PBS) under the management of M.K. King. The authors are grateful to Jason Taylor for his assistance with the drop tower experiments, Jignesh Maun for help with the filament pyrometry, and Dr. Sun Zhen for many suggestions on the numerical work.

## References

[1] J. Du, R.L. Axelbaum, Proc. Combust. Inst. 26 (1996) 1137–1142.
[2] H.K. Chelliah, C.K. Law, T. Ueda, M.D. Smooke, F.A. Williams, Proc. Combust. Inst. 23 (1990) 503–511.
[3] R. Chen, R.L. Axelbaum, Combust. Flame 142 (2005) 62–71.
[4] B.H. Chao, C.K. Law, J.S. T'ien, Proc. Combust. Inst. 23 (1990) 523–531.
[5] C.K. Law, Combust. Flame 24 (1975) 89–98.
[6] K. Mills, M. Matalon, Combust. Sci. Technol. 129 (1997) 295–319.
[7] D.L. Dietrich, J.B. Haggard, F.L. Dryer, V. Nayagam, B.D. Shaw, F.A. Williams, Proc. Combust. Inst. 26 (1996) 1201–1207.
[8] V. Nayagam, J.B. Haggard, R.O. Colantonio, A.J. Marchese, F.L. Dryer, B.L. Zhang, F.A. Williams, AIAA J. 36 (8) (1998) 1369–1378.
[9] K. Maruta, M. Yoshida, H. Guo, Y. Ju, T. Niioka, Combust. Flame 112 (1998) 181–187.
[10] S. Liu, B.H. Chao, R.L. Axelbaum, Combust. Fame 140 (2005) 1–23.
[11] S.W. Yoo, E.W. Christiansen, C.K. Law, Proc. Combust. Inst. 29 (2002) 29–36.
[12] S.D. Tse, D. Zhu, C.-J. Sung, Y. Ju, C.K. Law, Combust. Flame 125 (2001) 1265–1278.
[13] M.K. King, Proc. Combust. Inst. 26 (1996) 1227–1234.
[14] A. Atreya, S. Agrawal, Combust. Flame 115 (1998) 372–383.
[15] K. Mills, M. Matalon, Proc. Combust. Inst. 27 (1998) 2535–2541.
[16] E.W. Christiansen, S.D. Tse, C.K. Law, Combust. Flame 134 (2003) 327–337.
[17] P.B. Sunderland, R.L. Axelbaum, D.L. Urban, B.H. Chao, S. Liu, Combust. Flame 132 (2003) 25–33.
[18] P.B. Sunderland, D.L. Urban, D.P. Stocker, B.H. Chao, R.L. Axelbaum, Combust. Sci. Technol. 176 (2004) 2143–2164.
[19] V. Villimpoc, L.P. Goss, Proc. Combust. Inst. 22 (1988) 1907–1914.
[20] K.J. Santa, Z. Sun, B.H. Chao, P.B. Sunderland, R.L. Axelbaum, D.L. Urban, D.P. Stocker, Combust. Theor. Model. 11 (2007) 639–652.
[21] B.C. Connelly, S.A. Kaiser, M.D. Smooke, M.B. Long, Fourth Joint Meeting of the U.S. Sections of the Combustion Institute, Philadelphia, 2005.
[22] J.D. Maun, P.B. Sunderland, D.L. Urban, Appl. Opt. 46 (2007) 483–488.
[23] R.J. Kee, J.F. Grcar, M.D. Smooke, J.A. Miller, E. Meeks, A Program for Modeling Steady, Laminar, One-Dimensional Premixed Flames, Report SAND85-8240, Sandia National Laboratories, 1987.
[24] L.S. Rothman, C.P. Rinsland, A. Goldman, S.T. Massie, D.P. Edwards, J.-M. Flaud, A. Perrin, C. Camy-Peyret, V. Dana, J.-Y. Mandin, J. Schroeder, A. Mccann, R.R. Gamache, R.B. Wattson, K. Yoshino, K.V. Chance, K.W. Jucks, L.R. Brown, V. Nemtchinov, P. Varanasi, J. Quant. Spectrosc. Radiat. Transfer 82 (2003) 5–44.
[25] B.G. Carlson, K.D. Lathrop, in: H. Greenspan, C.N. Kelber, D. Okrent (Eds.), Computing Methods in Reactor Physics, Gordon and Breach, New York, 1968, pp. 171–266.
[26] J.F. Grcar, The Twopnt Program for Boundary Value Problems, Report SAND91-8230, Sandia National Laboratories, 1992.
[27] R.J. Kee, F.M. Rupley, J.A. Miller, Chemkin-II: A Fortran Chemical Kinetics Package for the Analysis of Gas Phase Chemical Kinetics, Report SAND89-8009B, Sandia National Laboratories, 1989.
[28] R.J. Kee, G. Dixon-Lewis, J. Warnatz, M.E. Coltrin, J.A. Miller, A Fortran Computer Code Package for the Evaluation of Gas Phase Multicomponent Transport Properties, Report SAND86-8246, Sandia National Laboratories, 1988.
[29] G.P. Smith, D.M. Golden, M. Frenklach, N.W. Moriarty, B. Eiteneer, M. Goldenberg, C.T. Bowman, R.K. Hanson, S. Song, W.C. Gardiner Jr., V.V. Lissianski, Z. Qin, available at http://www.me.berkeley.edu/gri_mech/.
[30] J.G. Quintiere, Fundamentals of Fire Phenomena, Wiley, New York, 2006, p. 277.
[31] F.A. Williams, Fire Safe. J. 3 (1981) 163–175.
[32] A. Macek, Flammability Limits: Thermodynamics and Kinetics, NBSIR Report 76-1076, National Bureau of Standards, Gaithersburg, MD, 1976.